AIAA 81-1340R

# Nonlinear Dynamic Simulation of a Tethered Aerostat

S.P. Jones* and J.A. Krausman†
*TCOM Corporation, Columbia, Md.*

**A nonlinear dynamic simulation computer program for a tethered aerostat has been developed and applied to the study of aerostat response to turbulence and other disturbances. The theoretical model includes a dynamic tether, dynamic motion of the ballonet air, and 6 degrees of freedom for the aerostat. Static and dynamic coefficients measured in a rotating-arm tow tank are employed and the equations of motion are written for a reference other than the mass center. A turbulence model using the Dryden power density spectrum was used to generate and prerecord turbulent winds which the program reads from a mass storage disk. In a study of aerostat response to turbulence, different "storms" of the same intensity gave the same statistical distribution of displacement and tether tensions. In a program verification study, the flight of an instrumented aerostat is compared with simulated flight having input winds reconstructed from measurements on the aerostat. The simulation duplicated the behavior of the real aerostat in most respects but with major exceptions, probably reflecting the inadequacy of the turbulence model in representing large wind fluctuations. Tether tension excursions were higher in the simulation indicating less damping in the model. Best results were obtained when longitudinal gradients of velocity were not taken into account.**

## Introduction

THE work described in this paper was motivated by the need for more detailed information about the dynamic response of tethered aerostats to atmospheric disturbances. Previous work on the dynamics of tethered aerostats has employed linearized stability models such as those of Redd et al.[1] and DeLaurier.[2,3] While these models provide insights into dynamic stability and, in the case of the latter, mean response to turbulence, they are limited to small perturbations and 3 degrees of freedom. The effect of aerodynamic nonlinearity, detailed motions and peak tether tensions under the influence of a time-dependent wind vector cannot be determined. The present paper describes a 6-degree-of-freedom, nonlinear dynamic simulation (NLDS) of a tethered aerostat and its application to the study of the TCOM 365 (365,000 ft$^3$). The theoretical model incorporates dynamic motion of the ballonet air after the model of DeLaurier,[4] a dynamic tether and a turbulence model based on MIL-F-8785B as interpreted by Chalk et al.[5]

The program has been used to study the response of tethered aerostats to turbulence as a tool for design and prediction of survivability. A major effort has been devoted to an experimental verification program, some of the results of which are reported.

## Theoretical Model

### Approach

The coordinate systems employed in the theoretical model, consisting of an Earth-fixed system (EFS) and a body-fixed system (BFS), are shown in Fig. 1. Initially the aerostat is in static equilibrium in a steady wind and the initial position is the origin of the EFS which has the $x$ axis oriented parallel to the wind vector. The origin of the BFS is the body reference point which is chosen to be the Archimedean Center of buoyancy. This has the advantage of being a fixed point for a particular aerostat but introduces nondiagonal terms in the mass matrix, as will be described.

In order to avoid confusion, vectors with components in the EFS will be denoted by primes. Thus the position of the aerostat at any time $t$ is given by the position vector $\boldsymbol{P}'$. The orientation is described by the Euler angles $\psi$, $\theta$, and $\phi$ and the direction cosine matrix $[C]$, which transforms from Earth to body coordinates. The aerostat's translational and angular velocities are represented by the column matrix

$$\{\eta\} = \{V, \Omega\} = \{U, V, W, P, Q, R\} \tag{1}$$

$$\boldsymbol{V} = [C]\dot{\boldsymbol{P}}' \tag{2}$$

The aerostat is subjected to a steady wind, $\boldsymbol{V}_s$, superimposed upon which may be a turbulence, $\boldsymbol{V}_t$, resulting in a relative velocity,

$$\boldsymbol{V}_r = \boldsymbol{V} + \boldsymbol{V}_s + \boldsymbol{V}_t \tag{3}$$

and a corresponding relative velocity column matrix $\{\eta\}_r$. In the turbulence model, to be detailed in a later section, $\boldsymbol{V}_t$ represents a "frozen field" such as described by Chalk et al.[5] When this model is used for free-flying aircraft it is assumed to be a stationary frozen field through which the vehicle translates. In the case of a tethered aerostat, which is restricted in translation, the field is assumed to be propagated with the velocity $\boldsymbol{V}_s$. This approach has been used by DeLaurier.[3]

It has been pointed out by Calligeros and McDavitt[6] and others[7,8] that for turbulence in the form of a traveling wave propagated along the $x$ axis with the velocity $U_s$, the acceleration of the wind relative to the aerostat does not contribute to the inertial forces.

$$\frac{\mathrm{d}}{\mathrm{d}t}\boldsymbol{V}_t = \frac{\partial \boldsymbol{V}_t}{\partial t} - U_s \frac{\partial \boldsymbol{V}_t}{\partial x} = 0 \tag{4}$$

Since $\boldsymbol{V}_s$ is constant with respect to time,

$$\dot{\boldsymbol{V}}_r = \dot{\boldsymbol{V}} \tag{5}$$

$$\{\dot{\eta}\}_r = \{\dot{\eta}\} \tag{6}$$

Presented as Paper 81-1340 at the AIAA Lighter-than-Air Systems Conference, Annapolis, Md., July 8-10, 1981; submitted July 21, 1981; revision received Oct. 27, 1981. 

*Advisory Scientist. Member AIAA.
†Senior Engineer.

This greatly simplifies the analysis. Now the equation of motion can be written in very general form,

$$0 = -[M]\{\dot{\eta}\} + \{\xi\} \tag{7}$$

in which the mass matrix $[M]$ represents the sum of real and apparent mass terms.

Equation (7) is integrated to obtain linear and angular velocities and the position vector $\boldsymbol{P}'$. The orientation in terms of Euler angles is found by integrating the relations given by Clark[9]:

$$\dot{\psi} = (Q\sin\phi + R\cos\phi)\sec\theta \tag{8}$$

$$\dot{\theta} = Q\cos\phi - R\sin\phi \tag{9}$$

$$\dot{\phi} = P + (Q\sin\phi + R\cos\phi)\tan\theta \tag{10}$$

For these relationships the Euler rotations must be in the order of $\psi,\theta,\phi$. After integration of Eqs. (8), (9), and (10), the transformation matrix $[C]$ is obtained by performing these rotations using yaw, pitch, and roll matrices, $[y]$, $[p]$, and $[r]$, respectively.

$$[C] = [r(\phi)]\,[p(\theta)]\,[y(\psi)] \tag{11}$$

The foregoing outlines the mathematical framework of the computer program. Remaining are the definitions of the real and apparent mass matrices, $[R]$ and $[A]$, and the computation of the force-moment matrix $\{\xi\}$.

#### Inertial Forces and Moments

Munk[10] has shown that the forces and moments on a body due to the acceleration of the fluid medium can be treated as if an additional or apparent mass were added to the body. That the apparent mass has a mass center or center of force is implicit in the work of Jones.[11] The kinetic energy approach of the latter can be used to derive the terms of the mass matrix $[A]$ such that

$$\{\mu\} = [A]\{\eta\}_r \tag{12}$$

where $\{\mu\}$ represents the momentum due to apparent mass.

The kinetic energy of the fluid, $T$, is given by

$$2T = m_1u_r^2 + m_2v_r^2 + m_3w_r^2 + I_{11}P^2 + I_{22}Q^2 + I_{33}R^2 - 2I_{12}PQ - 2I_{23}QR - 2I_{13}PR \tag{13}$$

where $m_1$, $m_2$, and $m_3$ are apparent masses for motion along the $x$-, $y$-, and $z$-body axes, respectively, and the $I$'s represent moments and products of inertia for rotations about these axes. Let $x$, $y$, $z$ be the location of the mass center in the BFS.

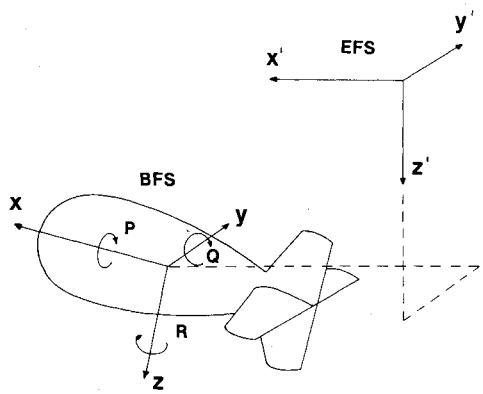


**Fig. 1 Coordinate systems for the theoretical model.**

Then,

$$u_r = U_r + Qz - Ry \tag{14}$$

$$v_r = V_r + Rx - Pz \tag{15}$$

$$w_r = W_r + Py - Qx \tag{16}$$

The terms of $[A]$ can be obtained from the relation

$$\mu_i = \frac{\partial T}{\partial(\eta_r)_i} = \sum_{j=1}^{j=6} A_{ij}(\eta_r)_j \tag{17}$$

For the computation of forces and moments it is convenient to express the momentum in terms of the translational and rotational momentum vectors, $\boldsymbol{h}$ and $\boldsymbol{k}$, representing the first three and last three terms of $\{\mu\}$, respectively. In these terms, the inertial forces and moments as given by Lamb[12] can be written

$$\boldsymbol{F}_{IA} = -\dot{\boldsymbol{h}} + \boldsymbol{F}_A \tag{18}$$

$$\boldsymbol{M}_{IA} = -\dot{\boldsymbol{k}} + \boldsymbol{M}_A \tag{19}$$

where

$$\boldsymbol{F}_A = \boldsymbol{h} \times \boldsymbol{\Omega} \tag{20}$$

$$\boldsymbol{M}_A = \boldsymbol{h} \times \boldsymbol{V}_r + \boldsymbol{k} \times \boldsymbol{\Omega} \tag{21}$$

However, a correction must be made to $\boldsymbol{M}_A$ for the fact that it contains terms representing the Munk destabilizing moment,[10] which are also contained in the aerodynamic coefficients. Denoting by $\boldsymbol{M}_{AC}$ the corrected moment vector,

$$\boldsymbol{M}_{AC} = \boldsymbol{M}_A - \begin{Bmatrix} (A_{22} - A_{33})VW \\ (A_{33} - A_{11})UW \\ (A_{11} - A_{22})UV \end{Bmatrix} \tag{22}$$

In column matrix notation, the components of $\boldsymbol{F}_A$ and $\boldsymbol{M}_{AC}$ are the first three and last three terms, respectively, of $\{\xi\}_A$ and Eqs. (18) and (19) can be written

$$\{\xi\}_{IA} = -[A]\{\dot{\eta}\} + \{\xi\}_A \tag{23}$$

Apparent masses and moments of inertia for the TCOM 365 aerostat were computed using the finite-element, source-panel method of Chow.[13] From this analysis the apparent mass center was found to be 1.4% of the hull length aft of the volumetric center of the hull.

The real mass matrix, $[R]$, can be derived in the same manner as $[A]$ if the masses, $m_i$, are replaced by $m$, the actual mass of the aerostat including the enclosed gases, $x,y,z$ is the location of the mass center in body coordinates, and $I_{ij}$ represents the actual moments and products of inertia. In addition, the velocity vector is that of the vehicle in inertial space, $V$. The combined effects are then,

$$\{\xi\}_I = -[A]\{\dot{\eta}\} - [R]\{\dot{\eta}\} + \{\xi\}_A + \{\xi\}_R \tag{24}$$

$$= -[M]\{\dot{\eta}\} + \{\xi\}_A + \{\xi\}_R \tag{25}$$

#### Aerodynamic Forces and Moments

Aerodynamic forces and moments are computed from experimentally measured coefficients obtained in a rotating-arm tow tank.[14] In measurements of this type the model has a rotational component of motion which makes possible the experimental determination of rotational stability derivatives as well as static coefficients. Measurements were made at

angles of attack $\alpha$ and sideslip $\beta$ from 0-360 deg, from which six static and six dynamic coefficients were obtained. The latter include lateral force and moment due to yaw rate, vertical force and pitching moment due to pitch rate and drag force due to both pitch rate and yaw rate. In addition, the coefficient of roll moment due to roll rate was computed assuming the fins to be the principal contributors to roll damping.

#### Buoyancy, Gravity, and Ballonet Slosh

Forces due to buoyancy and gravity can be found simply by transforming the Archimedean buoyancy and the weight from Earth to body coordinates. The former produces no moments about the reference point which is the center of buoyancy. For a fixed mass center $\boldsymbol{P}_G$ the gravitational force $\boldsymbol{F}_G$ produces the moment

$$\boldsymbol{M}_G = \boldsymbol{P}_G \times \boldsymbol{F}_G \tag{26}$$

Unfortunately for the analysis, however, owing to the mobility of the ballonet air, the center of mass moves dynamically and statically with changing orientation of the aerostat. The static position of the ballonet air's volumetric center, which is a function of ballonet design, air volume, and aerostat orientation is described elsewhere.[15] Ballonet curves giving this location as a function of volume and pitch angle are computed for each TCOM aerostat.

The equations of motion of the internal gases in the longitudinal plane have been derived by DeLaurier.[4] The formulation for the present case is similar to the latter's except that the spring constants are derived from the ballonet curves and the differential equation is adapted to the particular requirements of a three-dimensional simulation. Specifically the ballonet air is assumed to move dynamically only in the aerostat's longitudinal direction and to remain oriented with respect to the horizontal plane of the EFS. Integration of this equation gives the acceleration and mass center of the ballonet air and the helium to which it is directly coupled. The additional forces and moments on the aerostat are due to the acceleration reaction and the changing center of gravity affecting $\boldsymbol{M}_G$ and $[R]$.

#### Dynamic Tether

The tether model, depicted in part in Fig. 2, consists of $n$ straight elastic segments connected by universal joints or nodes at which the mass is assumed to be concentrated. The location of each node in the EFS is given by the vector $\boldsymbol{L}_i'$. The vector $\boldsymbol{L}_0$ in body coordinates is the fixed location of the confluence point or point of attachment to the aerostat and $\boldsymbol{L}_n'$ is the fixed location of the ground anchor point.

The equation of motion of the $i$th node is

$$-m_i \ddot{\boldsymbol{L}}_i' + \boldsymbol{T}_{i+1}' - \boldsymbol{T}_i' + \boldsymbol{G}_i' + \boldsymbol{D}_i' = 0 \tag{27}$$

The segment mass is $m_i$ and its gravitational force, $\boldsymbol{G}_i'$. The tension in a segment, $\boldsymbol{T}_i'$, is computed from the scalar length $l_i$, which has the unstretched value $l_0$, and the elastic constant $k_t$. In addition, the tether's internal damping is represented by the constant $\eta_t$.

$$\boldsymbol{l}_i' = \boldsymbol{L}_i' - \boldsymbol{L}_{i-1}' \tag{28}$$

$$T_i = k_t [l_i/l_0 - 1] + \eta_t \dot{l}_i / l_0 \tag{29}$$

Since the tension acts parallel to the segment,

$$\boldsymbol{T}_i' = (T_i/l_i)\boldsymbol{l}_i' \tag{30}$$

For the computation of aerodynamic drag, $\boldsymbol{D}_i'$, the segment is considered to be a cylinder on which the normal drag force is proportional to the square of the normal components of relative velocity,[16] which is taken to be that of the segment. Finally, the tether force and moment on the aerostat are due to the tension in the first segment transformed to body coordinates.

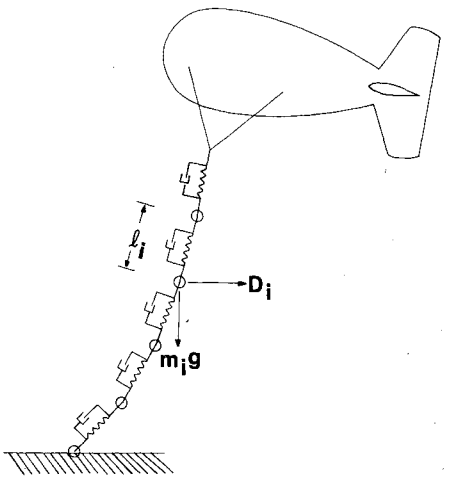


Fig. 2 Schematic of tether model.

The forces and moments in column matrix form due to real and apparent mass, velocity, buoyancy, gravity, and tether tension complete the computation of $\{\xi\}$ in Eq. (7).

## Turbulence Model

The frozen-field turbulence hypothesis of Taylor[17,18] using the von Kármán or Dryden power density spectra[19,20] has been formalized into a military specification for piloted aircraft.[5] This specification was used as a guide for the simulation of turbulence in the NLDS. The rms velocities for various levels of turbulence including a thunderstorm (21 ft/s) are specified.

Above an altitude of about 2000 ft the turbulence is assumed to be isotropic. For powered aircraft the frozen-field propagation velocity is taken to be that of the vehicle, which is large compared to the mean horizontal wind. For the present application it is assumed that the isotropic turbulence is superimposed on the steady wind $\boldsymbol{V}_s'$ and propagated with the velocity $\boldsymbol{U}_s'$.

In order to simulate the effect of turbulence, wind tables were prepared giving the three components of turbulence every second for 1000 s of simulated flight. Forty-six discrete wavelengths were selected and combined in random phase to simulate the continuous turbulence spectrum. The wavelengths were spaced at 10% intervals from 200 ft (one aerostat length) to 15,000 ft (about a storm cell size) and the amplitudes computed by integrating the Dryden power density spectrum over the interval. The three isotropic components contained the same wavelengths and amplitudes but were combined with their phases in a different random number sequence. By changing the phase relationships of the spectral components, various "storms" could be prepared and stored on a mass storage disk to be read by the NLDS program. Between the 1-s intervals of the table an interpolation routine was used.

Viewed from the aerostat, the turbulence is seen as fluctuations in velocity distributed in time, as read and interpolated from a disk file. Since the turbulence wave arrives at various stations at different times there will be a distribution of velocity along the longitudinal axis of the aerostat. If $t_r$ is the time of arrival at the reference point, a distance $\zeta_n$ from the nose, the turbulence seen by the nose is represented by the time

$$t_n = t_r + \zeta_n C_{11} / U_s \tag{31}$$

In an attempt to take the distribution of velocity on the aerostat into account, it is assumed that the wavelength of the turbulence is long compared to the aerostat and that the gradient of velocity is linear. The turbulence is read at five stations on the longitudinal axis and the mean value and gradient determined for each component by least squares. After transformation from Earth to body coordinates, the vertical component, for example, with respect to the longitudinal coordinate $\zeta$ is given by

$$W_t = \bar{W}_t + G_w \zeta \tag{32}$$

where $\bar{W}_t$ is the mean velocity of turbulence as seen at the reference point. The gradient $G_w$ is considered to have the same effect as a rotational velocity about the $y$ axis.

$$\frac{\partial W_t}{\partial \zeta} = G_w = -Q_t \tag{33}$$

The effect of the gradient on force and moment is taken into account by including $Q_t$ and $R_t$ as apparent angular velocities added to body rotations in $\{\eta\}_r$.

While this method of dealing with the distribution of velocity on the aerostat is flawed, particularly with respect to the long wavelength and linear assumptions, it is easily adaptable to the computer program in its present form. Another approach to this problem is that taken by Evans and DeLaurier[21] based on the panel method of Jones and DeLaurier.[8] The aerostat hull is divided into segments or panels along the longitudinal axis, on each of which the aerodynamic force can be computed. The fins are considered as separate panels. At any instant various panels will be subjected to different velocity vectors as the turbulence is propagated along the axis. This method has not yet been incorporated in the present simulation; however, it is an important subject for investigation about which more will be said in connection with the experimental study.

## Computer Program

The nonlinear dynamic simulation (NLDS) interfaces with an input program which computes steady-state data used as initial conditions, and an output program with data presentation and plotting routines. The input program, ordinarily used for steady-state performance analysis, permits input of atmospheric, configurational, lift, and altitude data from the computer keyboard. The output to a disk data file is read by the NLDS and provides the initial conditions as well as data on the weight, center of gravity, internal gas volumes, air density, tether length, altitude, and pitch angle.

Initially the program recomputes the equilibrium pitch angle and tether tension using the subroutines of the simulation program. With the equilibrium tether tension as the upper boundary condition, the tether model is integrated to find the ground anchor point consistent with static equilibrium. Although the recomputed anchor point will be slightly different from that of the input data, this procedure insures that the model starts in static equilibrium. If unperturbed, the model will undergo a damped oscillation with an initial amplitude in $x$ displacement of less than $10^{-7}$ ft.

**Table 1 Flight parameters for simulated response to turbulence**

| | |
|---|---|
| Aerostat weight | 11,070 lb |
| Hull volume[a] | 390,000 ft$^3$ |
| Standard gross lift | 18,950 lb |
| Tether weight | 0.409 lb/ft |
| Altitude | 8830 ft |
| Wind speed | 25 knots |
| Equilibrium pitch angle | 5.4 deg |

[a] Actual volume. Pattern volume = 365,000 ft$^3$.

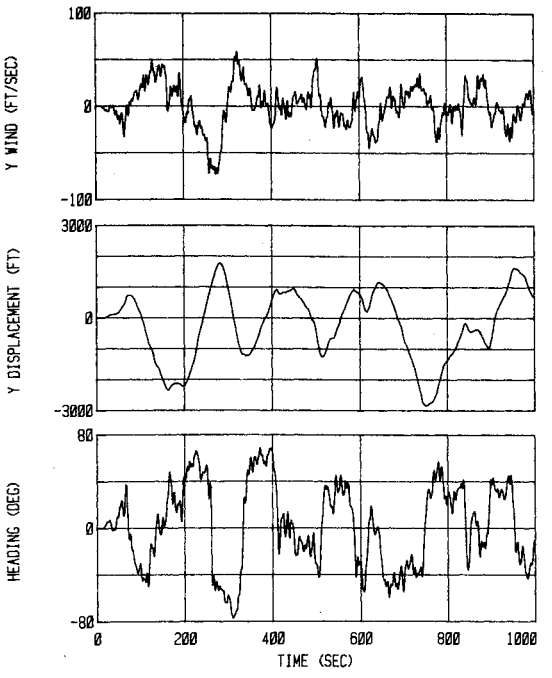


**Fig. 3 Lateral wind input and lateral response to 21-ft/s rms turbulence.**

The NLDS computes the total mass, moments of inertia, and terms of the mass matrix. These parameters are recomputed if the aerostat changes altitude by more than 100 ft. The program uses an Euler integration with a time step of 0.05 s for most applications. The wind vector can be computed from a time-dependent function or read from a mass storage data disk. The aerodynamic coefficients are read from a subroutine where they are represented by polynomials, curve fit from experimental data in 30-deg intervals of $\alpha$ and $\beta$.

Every 1 s of simulated flight time, data including position, orientation, and tether tension are output to a disk file. The output can also include other data such as angles of attack and sideslip, components of relative velocity, accelerations, position of the ballonet air mass, and coordinates of the tether elements. The data presentation program reads the output data file and can plot the results in one of several formats including a pictorial representation of the aerostat and its path in the $x$-$y$, $x$-$z$, or $y$-$z$ plane.

## Aerostat Response to Turbulence

Studies have been conducted to determine the response of TCOM aerostats to various levels of turbulence including thunderstorm intensity. As an example, the 365 described in Table 1 was subjected to isotropic turbulence having an rms value of 21 ft/s. The turbulence model previously described was used to generate the three components of turbulence, one of which is shown in Fig. 3. The flight duration was 1000 s. Space does not permit the presentation of all the data from this run; however, the lateral position and heading are plotted as a function of time in Fig. 3. The rms values of all the displacements and the tether tension are given in Table 2.

The lateral turbulence is representative of the longitudinal and vertical components although all are generated with different random number sequences and therefore the peak velocities vary and appear at different times. Note that the maximum velocity is about 70 ft/s, the maximum lateral displacement is 2800 ft and the heading changes by 80 deg.

Runs have been made with different "storms" in which the rms value of the turbulence is the same but the phases of the spectral components are in a different random number sequence. Although the aerostat motion is quite different, the

**Table 2 rms response of 365 aerostat to thunderstorm turbulence**

| Parameter | rms value |
|---|---|
| $x$ displacement | 1314.6 ft |
| $y$ displacement | 1168.2 ft |
| $z$ displacement | 481.7 ft |
| Pitch | 16.2 deg |
| Heading | 35.7 deg |
| Roll | 6.5 deg |
| Tether Tension | 5597.1 lb |

rms values and cumulative distributions of the displacements and tether tension tend to be the same. This is illustrated in Fig. 4, which shows the cumulative distribution of tether tension in 1-s intervals for four different 21-ft/s rms storms. The curve can be interpreted as the probability of a tension less than the stated value and is a valuable tool for designing tethers and estimating survival probability.

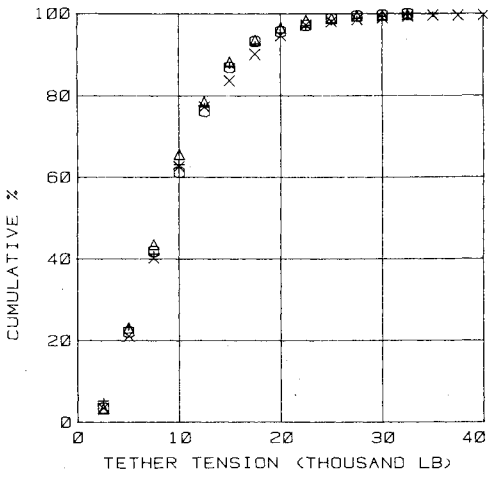


**Fig. 4 Cumulative distribution of tether tension for four 21-ft/s rms storms. Ordinate shows percent less than given tether tension.**

## Experimental Verification

In an effort to verify the NLDS program, a series of instrumented flights with a 365 tethered aerostat was undertaken at the TCOM Test Station on Grand Bahama Island. Instrumentation included pitch, roll, and heading gyros; a tether tension transducer; a number of directional anemometers at various locations on the aerostat; and a position locating system. The latter was capable of tracking the three-dimensional position of a transponder on the aerostat to an accuracy of about 1 ft. The digital telemetry output was recorded on magnetic tape so that the entire flight could be "replayed."

The anemometers, which measured velocity and direction in one plane, were mounted on 6-ft standoffs in front of the horizontal and vertical fins and midbody on the top and sides of the hull. Those at the top measured in the horizontal and on the sides in the vertical plane. They were of the Propvane type,‡ calibrated in windspeed and direction through the telemetry system according to manufacturer's specifications. The sensitivity to out-of-plane flow closely follows a cosine law.

There are many sources of error in attempting to measure a fluctuating wind field from a moving platform which itself interferes with the flow. Thus the most critical element of the experiments was the most prone to error. This fact should be taken into account when judging the results and comparison of real and simulated flight.

A computer program was written to subtract body motion from the wind data and transform it to a body-fixed coordinate system. It was assumed that the anemometers in front of the fins measured the freestream velocity. These velocities showed generally the same time profile as the midbody measurements but were displaced in time and an average of 12% less in magnitude. This was taken as the correction for accelerated flow near the hull. Since the midbody data were affected less by the angular velocity of the aerostat, they were used for the simulation runs. For this purpose the body-fixed data were transformed to an Earth-fixed system, the $x$ axis of which was parallel to the aerostat's initial and predominant direction. The aerostat's position and orientation were also transformed to the Earth-fixed system.

The data from several portions of flights were suitable for use in comparing the actual aerostat motion with the computer simulation. Table 3 gives the aerostat and flight parameters for one such study and the results are presented in Figs. 5-12. This particular flight was selected because it shows sufficient turbulence to cause significant aerostat motion and illustrates the effect of changes in wind direction. It is representative of the level of agreement of the simulation with the real aerostat motion in other flights.

**Table 3 Experimental verification flight parameters**

| | |
|---|---|
| Aerostat weight | 10,500 lb |
| Hull volume[a] | 390,000 ft$^3$ |
| Standard gross lift | 18,000 lb |
| Tether weight | 0.409 lb/ft |
| Altitude | 4050 ft |
| Wind speed | 14.3 knots |
| Equilibrium pitch angle | 5.6 deg |

[a] Actual volume. Pattern volume = 365,000 ft$^3$.

The wind inputs to the computer program were based on the turbulence model previously described. The average wind velocity in the $x$ direction of the EFS was 14.3 knots, which was taken to be the propagation velocity. The three components of wind with the average subtracted from the $x$ direction are shown in Fig. 5.

In comparing the computer simulation with the actual motions it was found that the use of apparent rotations as described in Eq. (33) gave exaggerated motions in the former. Much better comparisons were obtained by omitting the effect of the velocity gradient and considering the average velocity as computed for the five hull stations to be the velocity at the reference point. This point is illustrated by comparing Figs. 6 and 7. The former shows aerostat pitch with apparent rotation rates included and in the latter they have been omitted. The other comparisons are shown with this modification in the program.

In view of the probable inaccuracy of the turbulence model as applied to real winds, the actual and simulated motions are in reasonably good agreement. In particular the agreement of lateral displacement in Fig. 9 is excellent. Major departures in other motions are seen at 700-900 s which are probably due to a sudden change in the $x$ wind to about 40 ft/s from the reverse direction. During this same period there was a shift in the lateral wind. The model responded by charging forward and then overcompensating in the reverse direction (see Fig. 8), a behavior not seen in the real aerostat. At the same time the simulation turned through 360 deg while the real aerostat did not. These deviations probably result from the assumption that the velocity fluctuations are all propagated at a constant velocity in the same direction, which is almost certainly not true in the real world.

‡Manufactured by R.M. Young Company, Traverse City, Mich.

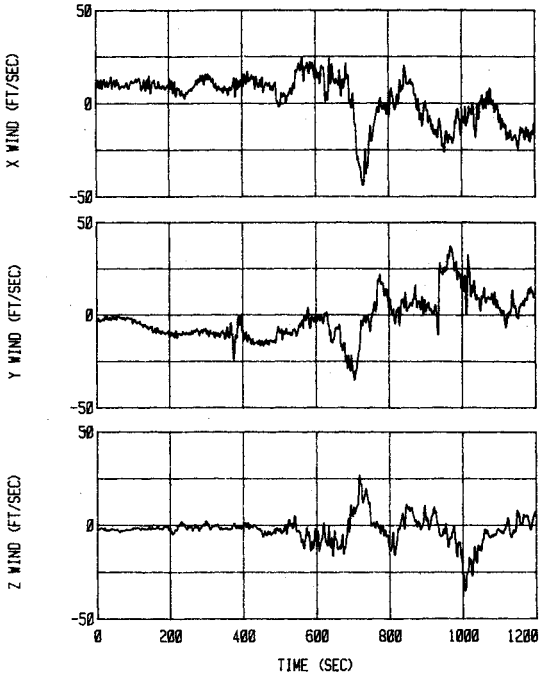


Fig. 5 Three components of experimentally measured winds.

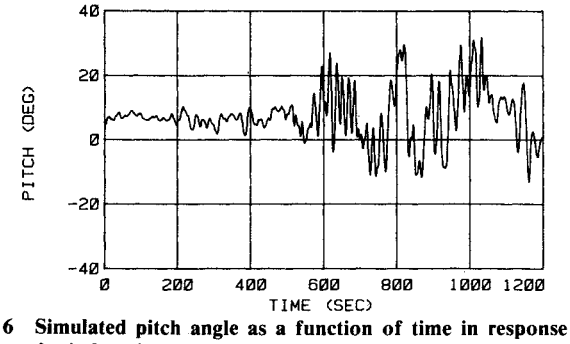


Fig. 6 Simulated pitch angle as a function of time in response to measured winds, with longitudinal velocity gradients represented by apparent rotation rates.

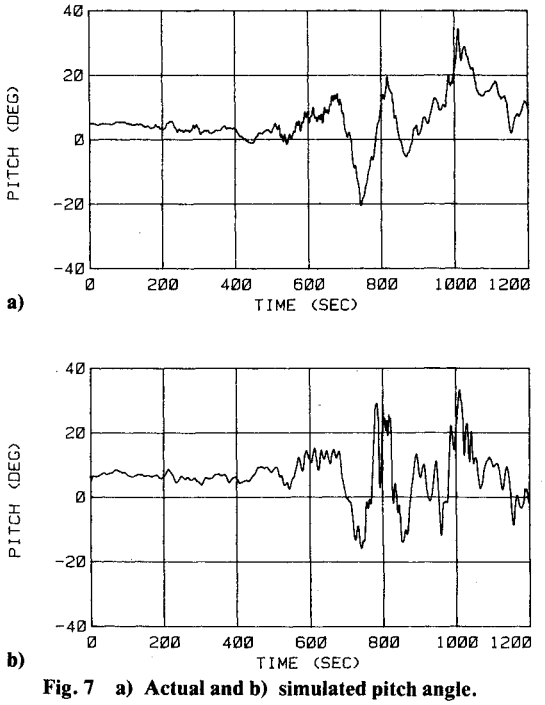


Fig. 7 a) Actual and b) simulated pitch angle.

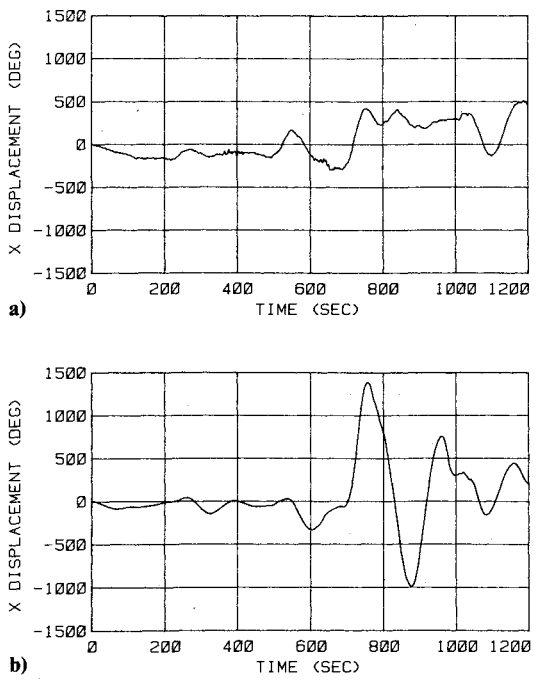


Fig. 8 a) Actual and b) simulated longitudinal displacement.

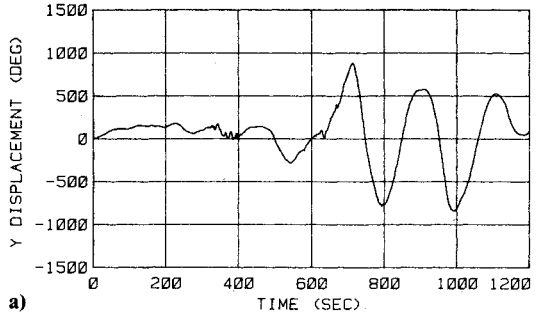


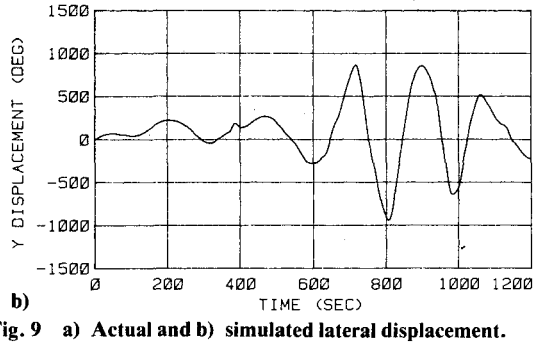


Fig. 9 a) Actual and b) simulated lateral displacement.

The events between 700 and 900 s, where the simulation shows the greatest deviation from reality, can best be understood by reference to Fig. 12, which is a pictorial presentation of the computer output. The aerostat is shown in a projection on the $x$-$y$ plane every 10 s, with a dot every 1 s of simulated flight. Referring to the $x$ direction as north, at 700 s the aerostat is heading NNW. The wind has shifted to the NW (negative $y$ component) and at the same time there is the onset of an updraft (positive $z$ component). The aerostat turns toward the NW and at the same time charges forward in response to the updraft. It will be recalled that the $x$ wind has a steady component of 14 knots or 24 ft/s, not shown in Fig. 5. In the seventh frame (770 s) the wind shifts toward the NE

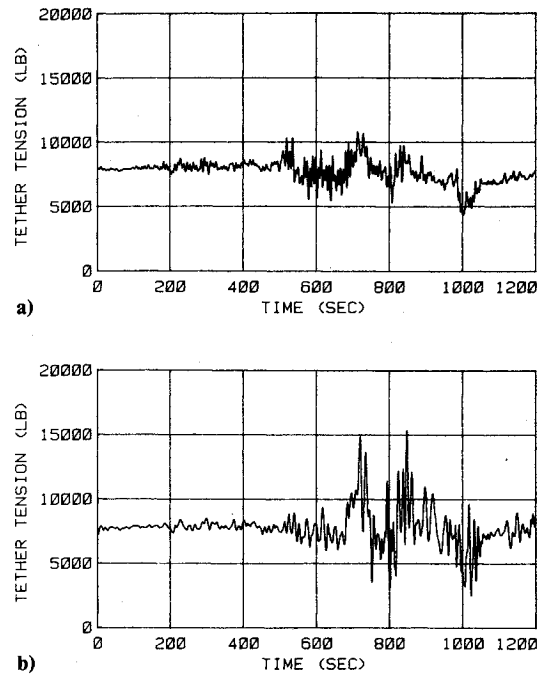


Fig. 10 a) Actual and b) simulated tether tension.

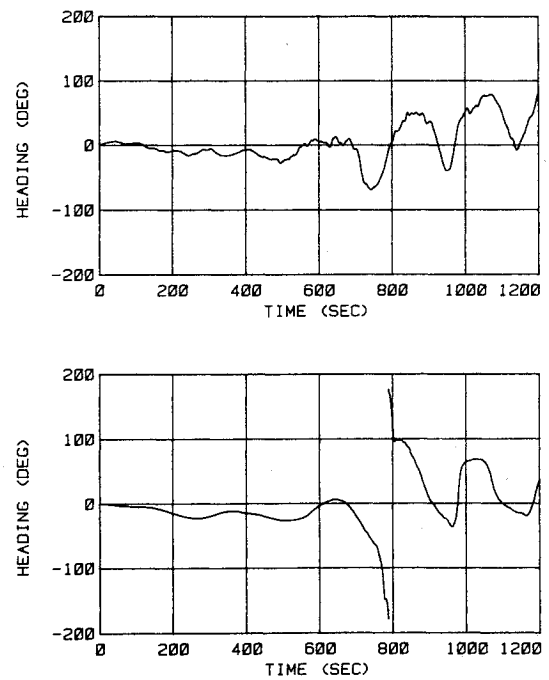


Fig. 11 a) Actual and b) simulated heading.

and the aerostat begins a turn in response. In the next three frames the wind shifts more to the north and the aerostat turns rapidly through 180 deg (apparent discontinuity in the heading). By frame 11 (810 s) the aerostat is heading east and drifts broadside to the wind for the next several seconds until it turns back into the prevailing north wind.

The real aerostat and the simulation were very nearly together at the beginning and ending of the period described. During the period their east-west displacements were almost the same, but the real aerostat turned to the NW and then back to the NE as the wind shifted.

In pitch (Fig. 7) the simulation duplicates the real motion to a reasonable degree in direction and magnitude. The simulated tether tension follows closely the same peaks as the

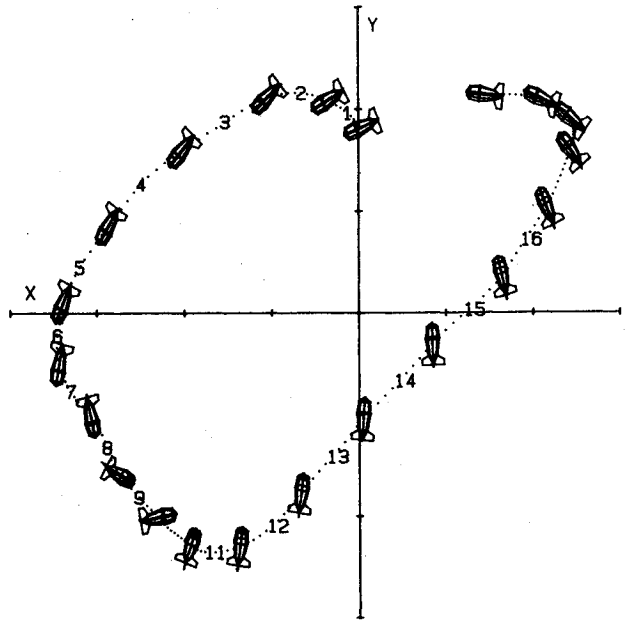


Fig. 12 Pictorial representation of aerostat simulated response to experimental winds from 700 to 900 s. View is a projection on the *x-y* plane.

real aerostat (Fig. 10) except that the excursions are much greater, indicating that the real system is more highly damped than the theoretical model. The simulation is thus conservative in predicting tether tensions.

## Summary and Conclusions

A 6-degree-of-freedom dynamic simulation of a tethered aerostat has been developed and programmed on a digital computer. Aerodynamic forces and moments are computed from experimental data obtained in a rotating-arm tow tank. These data include static and dynamic coefficients over a range of 360 deg in angles of attack and sideslip. The theoretical model incorporates a dynamic tether having elasticity, mass, and aerodynamic drag. Winds can be in the form of a time-dependent vector or as turbulence read from a disk file.

In an investigation of the response of aerostats to turbulence it was found that different "storms" of the same rms velocity give the same statistical distribution of displacements and tether tensions. Different storms are those in which the spectral components of the turbulence are in a different random phase relationship.

In a program verification study, experimental data were obtained for a series of instrumented aerostat flights. The wind data were reduced in such a way that they could be input to the computer simulation and the output compared with the motions of the real aerostat. From this study the following conclusions are drawn:

1) The computer simulation duplicates the behavior of a real aerostat to a reasonable degree, with significant exceptions when there are large shifts in wind direction. This could be due to inaccuracy of the turbulence model in representing real wind fields or possible error in the experimental measurement and reduction of wind data.

2) The simulation gave higher tether tension excursions than the real aerostat indicating that the latter is more highly damped than the dynamic tether model. In this respect the model is conservative when used as a design tool.

3) The use of apparent rotation rates to account for gradients of velocity on the aerostat gave exaggerated motions in the simulation. Better results were obtained when the average velocity over the hull was used. Further work is in-

dicated to test the panel method of representing the distribution of velocity.[8]

## Acknowledgments

The authors acknowledge the valuable contributions of M.S. Wheeler, who is principally responsible for the turbulence model, N.A. Dresner for reduction of the experimental flight data, and B.D. Sunkara for assistance with the computer program, simulation runs, and data plots.

## References

[1] Redd, L.T., Bland, R.M.B., and Bennett, R.M., "Stability Analysis and Trend Study of a Balloon Tethered in a Wind; with Experimental Comparisons," NASA TN D-7272, Oct. 1973.

[2] DeLaurier, J.D., "A Stability Analysis for Tethered Aerodynamically Shaped Balloons," *Journal of Aircraft,* Vol. 9, Sept. 1972, pp. 646-651.

[3] DeLaurier, J.D., "Predictions of Tethered-Aerostat Response to Atmospheric Turbulence," *Journal of Aircraft,* Vol. 14, April 1977, pp. 407-409.

[4] DeLaurier, J.D., "Influence of Ballonet Motions on the Longitudinal Stability of Tethered Aerostats," *Journal of Aircraft,* Vol. 17, May 1980, pp. 305-312.

[5] Chalk, C.R., Neal, T.P., Harris, T.M., Pritchard, F.E., and Woodcock, R.J., "Military Specifications—Flying Qualities of Piloted Airplanes," *Background Information and User Guide for MIL-F-8785B (ASG),* Air Force Flight Dynamics Laboratory, Air Force Systems Command, Wright-Patterson AFB, Ohio; see also AFFDL-TR-69-72, Aug. 1969.

[6] Calligeros, J.M. and McDavitt, P.W., "Response and Loads on Airships Due to Discrete and Random Gusts," Bureau of Aeronautics, Department of the Navy, Contract NOas 56-825-6; see also MIT, Cambridge, Mass., Tech. Rept. 72-1, Feb. 1958.

[7] Owens, P.R., "The Aerodynamics of Aircraft and Other Things," *Aeronautical Journal,* Vol. 77, Aug. 1973, pp. 383-404.

[8] Jones, S.P. and DeLaurier, J.D., "Aerodynamic Estimation Techniques for Aerostats and Airships," AIAA Paper 81-1339, July 1981.

[9] Clark, J.W., "Derivation and Application of Equations of Motion for Buoyant and Partially-Buoyant Air Vehicles," Department of the Navy, Air Vehicle Technology Department, VT-TM-1716, Feb. 1976.

[10] Munk, M.M., "Aerodynamics of Airships," *Aerodynamic Theory,* Vol. 6, edited by W.F. Durand, Julius Springer, Berlin, 1936, pp. 2-48.

[11] Jones, R., "Acceleration Derivatives in the Case of a Body Moving in an Ideal Fluid," ARC R&M 748, April 1921.

[12] Lamb, H., "Hydrodynamics," 6th ed., Dover Publications, New York, 1932, pp. 160-168.

[13] Chow, S.K., Hou, A.Y., and Landweber, L., "Hydrodynamic Forces and Moments Acting on a Body Emerging from an Infinite Plane," *The Physics of Fluids,* Vol. 19, Oct. 1976, pp. 1439-1449.

[14] Strumpf, A., "Rotating-Arm Model Experiments of Two TCOM Aerostats Tested With and Without Appendages," Stevens Institute of Technology, Davidson Laboratory, Rept. SIT-DL-78-9-2027 to TCOM Corp., Westinghouse Electric Corp., Dec. 1978.

[15] Jones, S.P., "Computation of Tethered Aerostat Pitch Angle and Vent Ceiling from Standard Curves," *Proceedings of the Tenth AFGL Scientific Balloon Symposium,* AFGL-TR-79-0053, Spec. Repts. 217, Air Force Geophysics Laboratory, March 1979, pp. 489-509.

[16] Hoerner, S.F. and Borst, H.V., *Fluid-Dynamic Lift,* Hoerner Fluid Dynamics, Bricktown, N.J., 1975, pp. 19-9, 19-10.

[17] Panofsky, H.A. and Press, H., "Meteorological and Aeronautical Aspects of Atmospheric Turbulence," *Progress in the Aeronautical Sciences,* Vol. 3, edited by A. Ferris, D. Kuchemann, and L.G.H. Sterne, Pergamon Press, New York, 1962.

[18] Lappe, U.O. and Davidson, B., "On the Range of Validity of Taylor's Hypothesis and the Kolmogoroff Spectral Law," *Journal of the Atmospheric Sciences,* Vol. 20, No. 6, Nov. 1963.

[19] Taylor, J., *Manual on Aircraft Loads,* Pergamon Press, New York, 1965.

[20] Houbolt, J.C., Steiner, R., and Pratt, K.G., "Dynamic Response of Airplanes to Atmospheric Turbulence Including Flight Data on Input and Response," NASA TR R-199, June 1964.

[21] Evans, J.R. and DeLaurier, J.D., "The Shenandoah Flies Again: A Computer Simulation," AIAA Paper 81-1325, July 1981.